PROCEEDINGS OF SCIENCE

Night Time Measurement of the UV Background by EUSO-Balloon

Š. Mackovjak[*1]**, A. Neronov**[1]**, P. Bobík**[2]**, M. Putiš**[2]**, L. Del Peral**[1, 3]**,**
M. D. Rodríguez Frías[1, 3, 8]**, K. Shinozaki**[4]**, C. Catalano**[5]**, J. F. Soriano**[3]**,**
G. Sáez-Cano[3]**, C. Moretto**[6]**, S. Bacholle**[7] **for the JEM-EUSO Collaboration**

[1] *ISDC - Data Centre for Astrophysics, University of Geneva, Switzerland*
[2] *Department of Space Physics, IEP, Slovak Academy of Sciences, Košice, Slovakia*
[3] *SPace & AStroparticle (SPAS) Group, UAH, Madrid, Spain*
[4] *Institute for Astronomy and Astrophysics, University of Tübingen, Germany*
[5] *Institut de Recherche en Astrophysique et Planétologie, CNRS-UPS Toulouse, France*
[6] *Laboratoire de l'Accélérateur Linéaire, Université Paris Sud, France*
[7] *Laboratoire AstroParticule et Cosmologie, Université Paris Diderot, France*
[8] *IFIC, CSIC, Dpto. Física Atómica, Molecular y Nuclear, Universitat de València, Spain*
E-mail: `simon.mackovjak@gmail.com`

A precise characterization of the Earth's UV background during night is essential for the observation of ultra-high-energy cosmic ray induced extensive air showers (EAS) from space. We have analyzed data from the flight of the EUSO-Balloon pathfinder mission that took place near Timmins (Canada) in the moonless night from 24 to 25 August 2014. The EUSO-Balloon telescope imaged the UV background in the wavelength range of 290 – 430 nm from an altitude of ~ 38 km with an 1 m^2 refractor telescope with $\sim 11^\circ$ field-of-view pointed in nadir direction. The UV data were complemented by the data of the Infrared camera onboard EUSO-Balloon, which was operating in the wavelength ranges of 10.37 – 11.22 μm and 11.57 – 12.42 μm. We have combined the UV and IR images to study the upward UV radiance from the Earth's surface and Earth's atmosphere. This allowed us to estimate the level of UV background in clear atmosphere conditions without man-made light and also to investigate the influence of clouds on the UV background. Comparison of the UV and IR images reveals an evident dependence of the upward UV radiance on the atmospheric conditions. This opens a possibility to use the UV albedo measurement for characterization of the cloud coverage. The efficiency of detection of EAS from space by EUSO like detectors varies depending on the level of the UV background. Using the available EUSO-Balloon data, we discuss the role of UV background variations due to clouds and man-made light on the exposure and effective area of EAS observations.

The 34th International Cosmic Ray Conference,
30 July – 6 August, 2015
The Hague, The Netherlands

[*] Speaker.

PoS(ICRC2015)685

1. Introduction

Ultra-High-Energy Cosmic Rays (UHECR) with energies of about 10^{20} eV are extremely rare events that can be detected only with experiments with large collection areas and long observation time. An order of magnitude increase of exposure, compared with present-days experiments, will be achieved by the Extreme Universe Space Observatory on-board the Japanese Experiment Module (JEM-EUSO) of the International Space Station (ISS), a next-generation space-based UHECR experiment [1]. JEM-EUSO will operate a refractive telescope with $\sim 60^\circ$ wide field-of-view (FoV) oriented in the nadir direction and monitoring a region of the Earth's atmosphere of the area of about 10^5 km^2 [2]. JEM-EUSO will use the atmosphere of the Earth as a giant high-energy particle calorimeter. It will measure the energy and arrival directions of UHECR via imaging the UV fluorescence light originating from the tracks of the UHECR-induced Extensive Air Showers (EAS) [3, 4]. The properties of the UV signal from EAS are determined by the properties of the EAS itself and by the transmission of the UV signal through the atmosphere. The UV light is strongly scattered in the atmosphere even in clear atmosphere conditions. Presence of clouds and aerosol layers further modifies the properties of the UV signal reaching the telescope [5]. Precise knowledge of the atmospheric conditions in the FoV of the JEM-EUSO telescope is, therefore, an important condition for the successful operation of the JEM-EUSO experiment.

A test of the operation of JEM-EUSO in cloudy atmosphere conditions was successfully performed during a first flight of the balloon-borne pathfinder mission of JEM-EUSO, EUSO-Balloon [6]. It observed a range of atmospheric conditions including clear moonless night atmosphere, clouds, and man-made lights from the altitude of approximately 38 km during about five hours of data taking. In the following we present the analysis of the UV imaging telescope data that are complemented with the Infrared Camera data. The dependences of UV background, which is constituted by the up-going reflection of the airglow, integrated star light, and zodiacal light [7] on atmospheric conditions are investigated and implications for the detection of EAS are discussed.

2. EUSO-Balloon First Flight

EUSO-Balloon is a mission of the French Space Agency CNES in coordination with the JEM-EUSO collaboration. The EUSO-Balloon measurements were performed during its first flight in nadir pointing mode in the time interval of 03:08 – 08:08 (UTC) on 25 August, 2014 within the period between two astronomical twilights. The main UV telescope of EUSO-Balloon consists of the refractive optics made of two Fresnel lenses with an ~ 1 m^2 area. On the focal plane, it is viewed by a photo-detector module (PDM) that is formed by 36 (6×6-array) multi-anode photomultiplier tubes (MAPMTs) with 8×8 pixels each. The PDM with 2304 pixels in total performs single photo-electron detection from an area of ~ 50 km^2. The MAPMTs are covered with band-pass filter that transmits UV photons with wavelength $\lambda \approx 290 - 430$ nm.

In this paper, we are using data obtained in the time interval 03:08 – 05:48 (UTC) while the detection setup was unchanged. The data were taken with a readout period of 2.5 μs, called gate time unit (GTU). They were organized in packets of 128 GTUs while the acquisition rate of the packets was ~ 19 Hz for the mode with the trigger generated by CPU clock and 20 Hz for the mode with acquisition generated by the clock board. During the observation time, two main goals were pursued. The first goal was detection of EAS-like events in the atmosphere generated by laser shots from a helicopter flying at a ~ 3.2 km altitude in the FoV of the UV telescope [8]. The other goal, which is the scope of this paper, was measurements of the properties of the UV background with spatial and temporal resolutions and sensitivity similar to those of JEM-EUSO. Apart from the main EUSO-Ballon telescope, an Infrared Camera (IRCAM) was operated throughout the flight with the acquisition rate $\sim 1/\,80$ s. It was used to monitor the atmospheric conditions in the FoV of the EUSO-Balloon telescope in the wavelength ranges of $10.37 - 11.22\,\mu$m and $11.57 - 12.42\,\mu$m. The full description of the mission and scientific payload can be found in Refs. [9, 10] and the general overview of the results from the first flight can be found in Ref. [11].

3. Results

3.1 Estimation of UV Background

Since EUSO-Balloon uses the refractive optics, the response of the UV telescope depends on wavelength and incident angle. For N_{pe} photoelectron observed by i-th pixel over an integration time Δt_{int}, the UV background intensity (I_{BG}) is expressed by

$$I_{\mathrm{BG}} \equiv \frac{N_{\mathrm{pe}}}{A_0 \int_{\varphi}\int_{\vartheta}\int_{\lambda} \kappa_i(\lambda, \vartheta, \varphi)\, f(\lambda)\, d\lambda\, \cos\vartheta\, d\vartheta\, d\varphi\, \Delta t_{\mathrm{int}}}, \tag{3.1}$$

where κ_i is the probability of producing a photoelectron by a photon on an entrance A_0 as a function of wavelength and incident direction, described as ϑ and φ on polar coordinates with respect to the optical axis. The function $f(\lambda)$ describes the relative abundance of incident photons within integrated wavelength band.

For the measurement of diffuse light like UV background in units of photons $\mathrm{m}^{-2}\,\mathrm{sr}^{-1}\,\mathrm{ns}^{-1}$, transmittance of lenses and the effective solid angle viewed by each pixel are leading factors to determine the effective area of each pixel. The function κ represents overall effects by these factors. To estimate this value, one needs to elaborate simulations of optics and detector response and an assumed model of UV background spectrum together with calibration efforts. In this paper, we approximate them by using the first calibration data for optics [12] and PDM [13, 14] together with detector simulations to present preliminary results for a relative background intensity.

The evolution of the measured I_{BG} throughout the duration of the exposure window 03:08:52 – 05:48:00 (UTC) is plotted in Fig. 1. The displayed values are relative to the mean value of UV background intensity over reference area "A" plotted in Fig. 2. The numerous sharp peaks in Fig. 1 represent intensive man-made UV lights in the FoV. Nearby city-light-free period starts only after $\sim$ 04:20 (UTC). Throughout this period, small variations of the intensity are presented due to a combined effect of man-made light (sharp peaks) and variations of atmospheric conditions (gradual changes).

We have used the imaging capabilities of the EUSO-Balloon telescope to produce a two dimensional plot of I_{BG} as a function of geographical coordinates. Using the reconstructed time evolution of the longitude, latitude, altitude and orientation of the telescope center [9] we calculated the geographical position of each pixel at each moment of the observation. The measured value of I_{BG} in each pixel was assigned to its calculated position on the 2D map. Measurements in

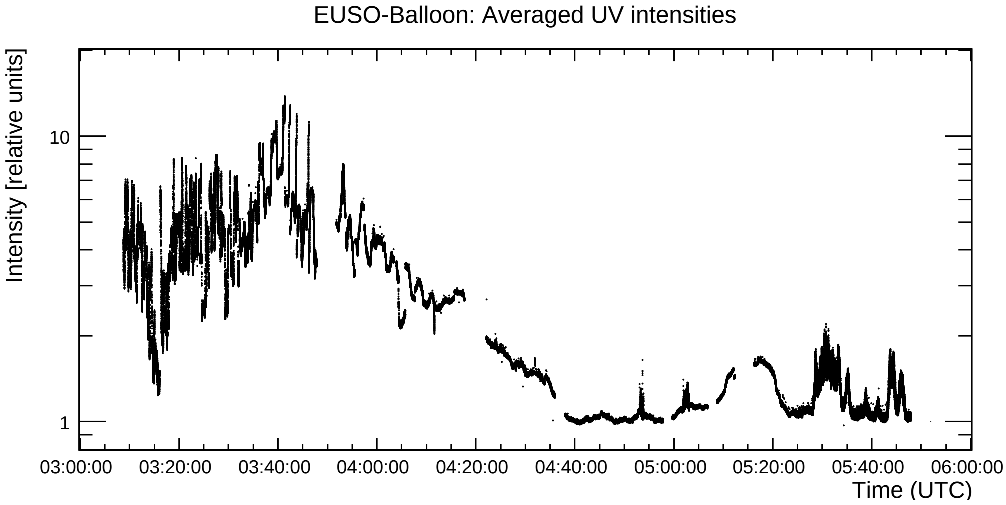

Figure 1: The measured and averaged UV intensities per 128 GTUs and per active calibrated pixels of whole PDM in time, in logarithmic scale. The displayed values are relative to the mean value of UV background intensity over reference area "A" plotted in Fig. 2.

each pixel of the 2D map were subsequently averaged in time. The resulting map is displayed in Fig. 2. To our knowledge, this is the first UV background imaging reconstructed by balloon-borne observations.

The brightest part of the map corresponds to the city lights of Timmins, with a detailed match of the brightest peaks to particular objects, such as mines, neighbouring towns, and the airport. Far away from Timmins, in the west part of the map, the intensity of the UV background is an order-of-magnitude lower. Still, gradual variations of the UV intensity are visible as gradations of blue in the map. To clarify the origin of variability of the UV background in the absence of man-made light, we have compared the UV map with the map of the infrared radiance obtained using the IRCAM, see Fig. 3. In clear atmosphere conditions, most of IR emission comes from the Earth in night time. The high-radiance features on the infrared map (gradations of yellow) correspond to the emission from objects on the Earth's surface. Lower radiance features are produced by emission from colder layers in the atmosphere and they correspond to clouds. Colder features are less sharp because of the motion of the clouds through the region on the time scale of data taking.

3.2 UV Background in Different Atmospheric Conditions

The first flight of EUSO-Balloon offers various scenes observed in the UV band. Indeed, we do not observe large variations in the UV background intensity from different ground surfaces, such as grass, forest, and lakes. The intensities of the UV radiation from pixels with different surfaces are almost unchanged. The influence of clouds is more significant and their presence increases the intensity of the UV background. In general, there is an anti-correlation between the UV intensity from a given direction and the IR radiance from the same direction as it can be seen by comparison of the UV and IR maps in Figs. (2, 3) and also directly in Fig. 4. Pixels with the lowest UV intensity and the highest IR radiance correspond to clear atmosphere. For these pixels, there is no (anti)correlation between the UV and IR intensities. The spread of the IR flux is determined by the

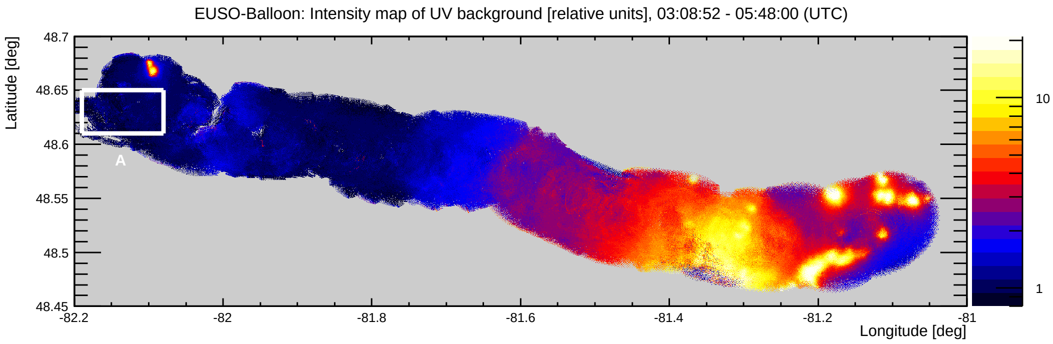

Figure 2: The intensity map of UV background in logarithmic scale. The bright areas with high intensities represent artificial light in the city Timmins with neighborhoods, mines, and airport. The red and light blue areas are related to cloud coverage. The dark blue areas indicate the lowest values of UV background. The displayed values are relative to the mean value of UV background intensity over reference area "A".

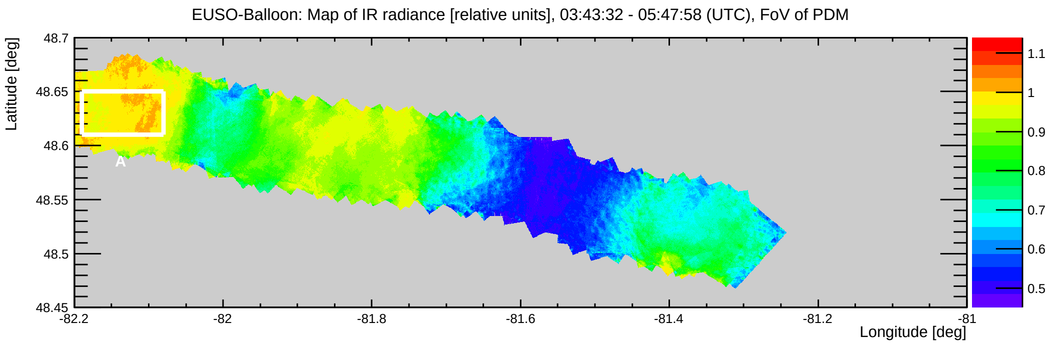

Figure 3: The map of IR radiance is created by plotting averaged values for particular positions. The absolute values were changing in time due to the movement of clouds and the motion of EUSO-Balloon. The displayed values are relative to the mean value of IR radiance over reference area "A".

spread of the IR radiances of regions on Earth's surface.

Adjacent to the clear atmosphere scene, there is a clear anti-correlation branch of UV and IR radiation in the UV intensity range of $\sim 0.8-2$ in relative units. Qualitative interpretation for the anti-correlation is that clouds with higher optical depth have higher albedo which increases the overall intensity of the UV background. Furthermore, UV radiation is absorbed in the atmosphere and higher altitude clouds can have higher albedo (at equal optical depth). Higher clouds are also colder and produce lower IR radiance. The variation of reflected solar UV radiation from the ground and clouds during the day is well known [15], but for night time UHECR detection purposes, it must be characterized with high precision.

Reconstruction of the properties of UHECR flux from the EAS data collected by a space-borne fluorescence telescope like JEM-EUSO requires a detailed characterization of the properties of the atmosphere in the FoV of the telescope. The combination of the IR and UV data plotted in Fig. 4 provides a powerful tool for such characterization. It opens the possibility to assign individual pixels with clear atmosphere conditions and mask the cloudy pixels and pixels affected by man-made light. It also allows to characterize the cloud coverage in the cloudy pixels and it opens the possibility to use the EAS data taken in the cloudy atmosphere conditions. Groups of pixels

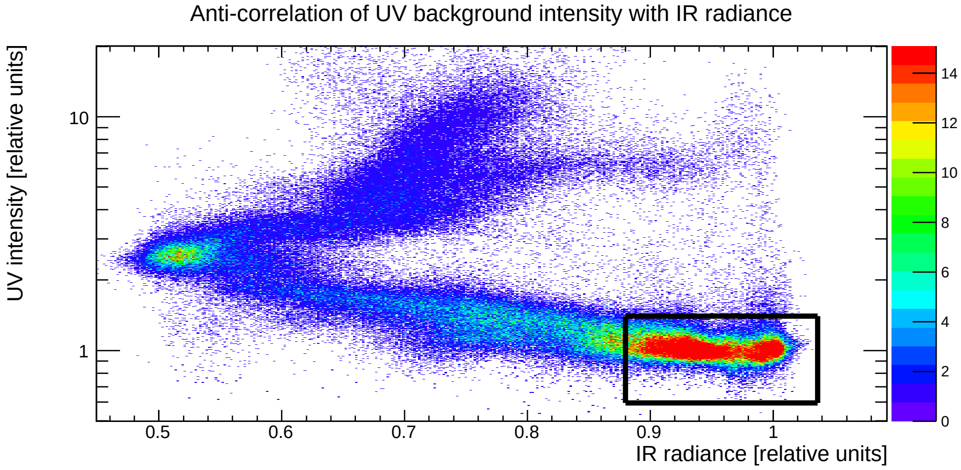

Figure 4: The cross-correlation of IR radiances and UV intensities of all pixels from the UV and IR map. The color scale represents the number of overlapping pixels in the scatter plot. The selected box represent conditions that are most efficient for the detection of EAS.

affected by man-made lights are clearly visible in Fig. 4 while they do not follow the general IR-UV anti-correlation. Clear atmosphere pixels are the "mainland" of the low UV – high IR flux. The cloudy atmosphere pixels are situated along the anti-correlation branch.

EAS data taken in the clear atmosphere regions provides the highest quality data. Using the data of EUSO-Balloon we estimated the fraction of the clear atmosphere regions over the all observed area. We tentatively define this highest quality region to consist of the pixels falling within the black box displayed in Fig. 4 (for illustrative purposes). The "clear atmosphere" box contains $\sim 25\%$ of all pixels from the observed area. This is in agreement with the cumulative fraction of pixels with I_{BG} above a threshold that is presented in Fig. 5 and indicates fraction of area with the value of UV background lower than the threshold value. In a more detailed approach, the "best quality" box has to be determined based on the requirements for the quality of the UHECR data (which is beyond the scope of this analysis). For example, taking data at the same UV background intensity but with lower IR introduces events in cloudy pixels. This should not affect the energy threshold for the UHECR events, but introduces an uncertainty of energy estimation related to possible uncertainties of the cloud properties. We note, that we expect to observe different ratios of UV and IR radiation depending on the location and the season.

In general, combination of the measurements of IR emission and UV albedo of the clouds provides a tool for characterization of the clouds, which will improve the quality of the reconstruction of EAS occurring in the cloudy conditions. This tool is complementary to the tools for retrieval of the cloud-top height [16, 17] and optical depth of clouds [18] from the IRCAM data alone [19]. However, detailed studies of physical parameters of the atmosphere that affects the variation of the UV background are beyond the scope of this contribution.

4. Conclusions

The first flight of EUSO-Balloon offered high-quality data for the investigation of UV background for observations of EAS from the top of the atmosphere and/or from space. We have ana-

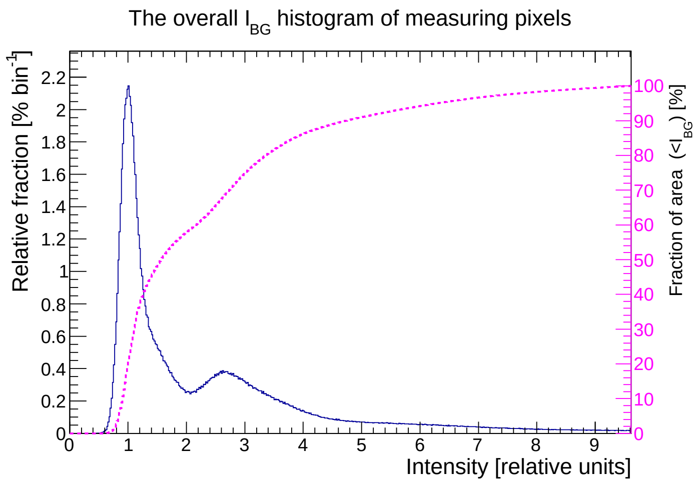

Figure 5: The overall histogram filled with all measured values along with cumulative fraction above the threshold I_{BG} that represent fraction of area with I_{BG} lower than the threshold value.

lyzed UV and IR data from a 3 hours exposure of EUSO-Balloon and produced maps of UV and IR radiation from the Earth's surface and atmosphere in the FoV of the UV telescope. We have presented relative variation of UV background in different atmospheric conditions. Cross-correlation of the UV and IR maps has allowed to detect the phenomenon of the night-time UV albedo of clouds. Anti-correlation between IR radiance and UV intensity in individual pixels of the maps is explained by this phenomenon. We have shown that a combination of the IR and UV data on pixel-by-pixel basis provides a tool for masking the regions affected by clouds and city light in the FoV. This tool is essential for selection of high-quality cosmic ray data. This first study of the UV background for the JEM-EUSO mission will be improved, systematic uncertainties will be specified and absolute values of the UV background will be released. The study will be also developed with future flights of EUSO-Balloon scheduled for 2017 [20], with the ground-based pathfinder EUSO-TA [21] and with Mini-EUSO pathfinder planned for installation at the International Space Station.

Acknowledgment: Š. Mackovjak acknowledges support from the Swiss Government via Swiss Government Excellence Scholarships for Foreign Scholars and Artists for the Academic Year 2014 – 2015. This work was partially supported by Basic Science Interdisciplinary Research Projects of RIKEN and JSPS KAKENHI Grant (22340063, 23340081, and 24244042), by the Italian Ministry of Foreign Affairs, General Direction for the Cultural Promotion and Cooperation, by the 'Helmholtz Alliance for Astroparticle Physics HAP' funded by the Initiative and Networking Fund of the Helmholtz Association, Germany, and by Slovak Academy of Sciences MVTS JEM-EUSO as well as VEGA grant agency project 2/0076/13. Russia is supported by the Russian Foundation for Basic Research Grant No 13-02-12175-ofi-m. The US is supported by the NASA grants NNX13AH55G, NNX13AH53G. The Spanish Consortium involved in the JEM-EUSO Space Mission is supported by the Spanish Government MICINN & MINECO under projects AYA2009-06037-E/AYA, AYA-ESP 2010-19082, AYA2011-29489-C03-01 and AYA2011-29489-C03-02, AYA-ESP2012-39115-C03-01 and AYA-ESP2012-39115-C03-03, AYA-ESP 2013-47816-C4, MINECO/FEDER-UNAH13-4E-2741, CSD2009-00064 (Consolider MULTIDARK) and by Comunidad de Madrid under projects S2009/ESP-1496 & S2013/ICE-2822. The calculations were performed by SPAS-UAH Cluster. M. D. Rodríguez Frías acknowledges the SNSF for a Sabbatical research stay at the University of Geneva and a grant under the "Atraccio de Talent" program, Universidad de Valencia. L. del Peral acknowledges a senior grant for a Sabbatical stay at University of Geneva from the Spanish Ministerio de Educación, Cultura y Deporte.

References

[1] J. H. Adams Jr. et al. - JEM-EUSO Collaboration, *Astroparticle Physics* **44** (2013) 76

[2] M. Casolino et al. - JEM-EUSO Collaboration, *Experimental Astronomy* (2014), to be printed

[3] M. Bertaina et al. - JEM-EUSO Collaboration, *Experimental Astronomy* (2014), to be printed

[4] S. Biktemerova et al. - JEM-EUSO Collaboration, *Experimental Astronomy* (2014), to be printed

[5] A. Guzmán et al. - JEM-EUSO Collaboration, *Experimental Astronomy* (2014), to be printed

[6] P. von Ballmoos et al. - JEM-EUSO Collaboration, *Advances in Space Research* **53** (2014) 1544

[7] C. Leinert et al., *Astronomy and Astrophysics Supplement Series* **127** (1998) 1

[8] J. Eser et al. - JEM-EUSO Collaboration, *Proc. 34th Int. Cosmic Ray Conf.* , # 0860 (2015)

[9] P. von Ballmoos et al. - JEM-EUSO Collaboration, *Proc. 34th Int. Cosmic Ray Conf.* # 0725 (2015)

[10] M. D. Rodriguez Frias et al. - JEM-EUSO Collaboration, *Proc. 34th Int. Cosmic Ray Conf.* # 1309 (2015)

[11] M. Bertaina et al. - JEM-EUSO Collaboration, *Proc. 34th Int. Cosmic Ray Conf.* # 0890 (2015)

[12] C. Catalano et al. - JEM-EUSO Collaboration, *Proc. 34th Int. Cosmic Ray Conf.* # 0717 (2015)

[13] C. Moretto et al. - JEM-EUSO Collaboration, *Proc. 34th Int. Cosmic Ray Conf.* # 1016 (2015)

[14] S. Dagoret et al. - JEM-EUSO Collaboration, *Proc. 34th Int. Cosmic Ray Conf.* # 0625 (2015)

[15] T. F. Eck et al., *Journal of Geophysical Research* **92** (1987) 4287

[16] A. Merino et al. - JEM-EUSO Collaboration, *Proc. 34th Int. Cosmic Ray Conf.* # 0979 (2015)

[17] I. Tabone et al. - JEM-EUSO Collaboration, *Proc. 34th Int. Cosmic Ray Conf.* # 0889 (2015)

[18] G. Sáez-Cano et al. - JEM-EUSO Collaboration, *Proc. 34th Int. Cosmic Ray Conf.* # 1024 (2015)

[19] J. F. Soriano et al. - JEM-EUSO Collaboration, *Proc. 34th Int. Cosmic Ray Conf.* # 1008 (2015)

[20] L. Wiencke et al. - JEM-EUSO Collaboration, *Proc. 34th Int. Cosmic Ray Conf.* # 0816 (2015)

[21] L. W. Piotrowski et al. - JEM-EUSO Collaboration, *Nuclear Instruments and Methods in Physics Research* **A773** (2015) 164